Available online at www.sciencedirect.com
SCIENCE DIRECT®
Chemical Physics 292 (2003) 477–485
Chemical Physics
www.elsevier.com/locate/chemphys

The Disk Chopper Spectrometer at NIST: a new instrument for quasielastic neutron scattering studies

J.R.D. Copley[a,*], J.C. Cook[a,b]

[a] NIST Center for Neutron Research, National Institute of Standards and Technology, 100 Bureau Drive, Gaithersburg, MD 20899-8562, USA
[b] Department of Materials and Nuclear Engineering, University of Maryland, College Park, MD 20742, USA

Received 22 October 2002; in final form 14 March 2003

Abstract

We describe the Disk Chopper Spectrometer (DCS) at the NIST Center for Neutron Research (NCNR). The maximum measured flux at the sample, averaged over the 3 cm width and 10 cm height of the beam, with all choppers turning at 20,000 revolutions per minute and phased to transmit neutrons through the widest slots on each disk, is approximately 3×10^4 n cm^{-2} s^{-1}. In this configuration the elastic resolution FWHM (full width at half maximum height) with an incident wavelength of 6 Å is 67 μeV. In an alternative configuration, achieved by changing the chopper phases so that neutrons pass through somewhat narrower slots, the elastic resolution FWHM at 6 Å is 34 μeV. Useful wavelengths range from about 1.5 Å to at least 12 Å. The DCS has been used for a variety of measurements, including quasielastic neutron scattering (QENS) studies of systems such as water in confined geometries and biological molecules in solution.

1. Introduction

According to a recent US Government report [1] the NIST Center for Neutron Research (NCNR), located at the Gaithersburg campus of the National Institute of Standards and Technology (NIST), is currently the "highest performing and most used neutron facility in the United States". Its neutron source is a 20 MW research reactor with a split core, designed so that the radial beam tubes do not directly view the fuel. All of the instruments in the NCNR neutron guide hall view a recently commissioned state-of-the-art liquid hydrogen cold source [2]. The inelastic scattering instruments in the guide hall include a spin-echo spectrometer [3], a backscattering spectrometer [4], a three-axis spectrometer, and the Disk Chopper time-of-flight Spectrometer (DCS).

2. The spectrometer

The DCS is a direct geometry machine, in many respects similar to IN5 at the Institut Laue–Langevin (Grenoble, France) [5], "Mibemol" at

* Corresponding author. Tel.: +1-301-975-5133; fax: +1-301-921-9847.
E-mail address: john.copley@nist.gov (J.R.D. Copley).

0301-0104/03/$ - see front matter © 2003 Elsevier Science B.V. All rights reserved.
doi:10.1016/S0301-0104(03)00124-1

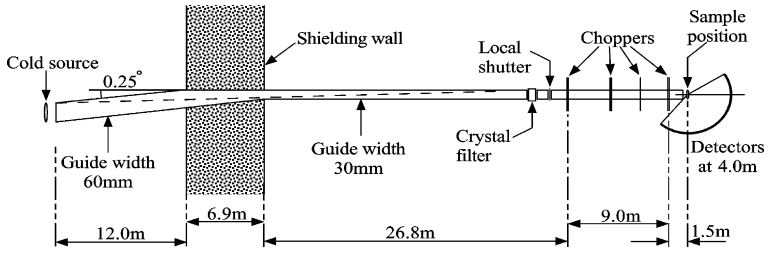

Fig. 1. An overall schematic plan view of the DCS.

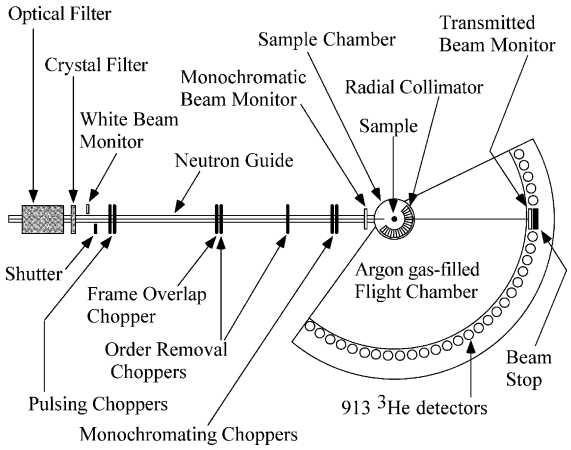

Fig. 2. A more detailed plan view of the DCS.

the Laboratoire Léon Brillouin (Saclay, France) [6], and NEAT at the Hahn–Meitner Institut (Berlin, Germany) [7]. It employs multiple choppers to produce a pulsed monochromatic beam at the sample position, and time-of-flight analysis of events in a large array of detectors to determine energy transfers E and wave vector transfers $\mathbf{Q}$ for neutrons scattered by the sample. An overall plan view of the instrument is shown in Fig. 1 and a more detailed view appears in Fig. 2.

2.1. Beam filters

A customized "neutron optical filter" removes high energy neutrons and gamma radiation from the beam. This device crudely approximates a curved guide but has the advantage that at relatively short wavelengths the beam at the exit remains uniformly bright [8]. It comprises a 6.9 m long asymmetric tapered section followed by a parallel guide that is offset 0.25° with respect to the initial beam direction. The downstream guide is 30 mm wide and 100 mm tall; the upstream width and height are 60 and 150 mm respectively. To remove the remaining small but significant flux of epithermal neutrons with wavelengths close to 0.55 Å [9] we use a crystal filter made from blocks of pyrolytic graphite oriented with their c axes parallel to the beam direction and cooled to $\approx$90 K. The length of the filter (in the beam direction) is 100 mm.

2.2. The choppers and the channeled guide

After the graphite filter, and following a local beam shutter, the guide proceeds through seven disk choppers in four housings. The guide is continuous apart from 20 mm guide cuts that accommodate each of the disks. The guide and four chopper housings share a common vacuum. The first and fourth housings contain counter-rotating pairs of choppers that pulse and monochromate the beam. The intermediate choppers remove orders and reduce the number of pulses at the sample to minimize frame overlap. In these respects the DCS and NEAT designs are quite similar.

Each of the disks in the first and fourth chopper housings has three slots. The angular locations of the slots on a given pair of disks are such that by suitably choosing the relative phase of the two choppers we can select a single pair of slots of identical width, one on each disk, that transmit neutrons. Since burst time varies with slot width, this design allows the user to choose among three distinct intensity/resolution conditions without having to change the wavelength or the speed of the choppers. A closely related aspect of this

design is that from the first chopper to its exit the guide is internally fitted with sets of reflecting glass plates, creating vertical channels that restrict the lateral motion of neutrons as they pass down the guide. The idea is to optimize intensity at the sample, to the extent that this is feasible, for the three intensity/resolution conditions corresponding to the three distinct choices of slot width in the pulsing and monochromating chopper disks [10]. The guide that passes through the choppers, originally constructed using four internal sets of plates, was recently modified by removing the inner two sets of plates, creating three channels rather than the original five [11]. The measured gains are substantial, the instrumental resolution is unchanged, and there is no increase in the background.

The choppers can be operated at any speed ω_0 between 1200 and 20,000 revolutions per minute. Typically six of the seven choppers run at their maximum speed and the remaining chopper (the "frame overlap chopper") is operated at the same speed or at $\omega_{FO} = \omega_0(m-1)/m$ where $m > 1$ is a small integer. The corresponding frequency of pulses at the sample is either ω_0 or ω_0/m. The long term root mean square phase instability of the choppers is $\approx$100 ns at their maximum speed.

2.3. The sample chamber, flight chamber, and detectors

The guide continues after the final chopper housing and then enters the sample chamber. The effective inside diameter of the sample chamber is 736 mm, sufficient to accommodate the majority of sample environment devices. A short guide section within the sample chamber may be removed if desired. We normally operate with an oscillating radial collimator whose purpose is to minimize scattering from the sample environment without significantly reducing scattering from the sample [12]. The collimator is easily lowered below the beam if circumstances warrant such action in order to accommodate a large piece of equipment. The sample chamber is accessible from the side through an opening that is 0.48 m wide and 1.61 m high, as well as from an upper level platform that is 1.44 m above beam center line. A gas-handling system affords the possibility to replace the air in the sample chamber with a gas that scatters much more weakly, such as argon.

A thin (0.08 mm) aluminum window separates the sample chamber from the flight chamber. The flight chamber is filled with argon at a very slight overpressure, typically 1–4 Pa, and a single sheet of ultrathin (0.009 mm) aluminum acts as its outer window. Just outside the window there are 15 racks that together hold 913 detectors, each of which is located with its central wire 4010 mm from the sample center. The detectors have an active volume of ^{3}He at 600 kPa (100 kPa $\approx$ 1 atmosphere), 400 mm long, 31 mm wide, and 12 mm thick. The detectors are arranged in three banks. The middle bank comprises 325 detectors ranging in scattering angle 2θ from $-30°$ to $-5°$ and from 5° to 140°. The upper and lower banks, located 531 mm above and below the scattering plane, comprise 294 detectors apiece, ranging from $-30°$ to $-10°$ and from 10° to 140°. There are no gaps within these angular ranges (other than those due to the upper and lower detectors being tangent to Debye–Scherrer rings); at $2\theta > 30°$ the angular separation of adjacent detectors in all three banks is approximately 0.5°.

2.4. Data acquisition and data reduction

The data acquisition system time-stamps individual events in 930 signal input channels employing up to 1024 time channels. The signal inputs currently accommodate the 913 ^{3}He detectors, four beam monitors and a 120 Hz pulser. The remaining inputs are available for additional detectors, beam monitors, and/or logic signals that are correlated with the choppers. For each of the input channels the number of counts in each time channel is stored as an individual datum in memory and this information is written to disk at regular intervals. Since there is no hardware grouping of signal inputs, data from individual detectors can be eliminated with no loss of valid data. Each of the 1024 time channel widths can be individually specified within the software in multiples of 50 ns, which is the basic resolution of the data acquisition system. Histogram periods can be as long as 50 ms, which is the maximum possible value of the

time T_S between pulses at the sample. Thus data can be binned in time channels of equal width (typically $T_S/1000$), in time channels of unequal width such that the width in energy transfer is approximately constant, or in any other scheme that is consistent with the design of the data acquisition system. The histogram channel counter reset time, relative to the mean time of arrival of neutrons at the sample, can be freely defined in software.

Reduction, visualization and analysis of DCS data are generally performed using a software package called DAVE (''Data Analysis and Visualization Environment''), which is written in the IDL language.[1] Source code and binary executables are available on the Web at http://www.ncnr.nist.gov/dave/.

3. Performance

The intensity at the sample, measured with all choppers turning at their maximum speed, is shown in Fig. 3 as a function of incident wavelength λ. The corresponding FWHM (full width at half maximum height) elastic resolution is shown in Fig. 4. Results are shown for two of the three possible intensity/resolution conditions. These conditions correspond to chopper phasings that transmit neutrons through the widest slots and the medium width slots. They are known as the ''low resolution'' and ''medium resolution'' conditions respectively. The resolution width for the third condition, which employs the narrowest slots and is known as the ''high resolution'' condition, is typically about half the width for the medium resolution condition at the same wavelength. To date the high resolution mode has not been used; the intensity is at least an order of magnitude less than the ''medium resolution'' intensity at the same wavelength.

With reference to Fig. 3 beam-averaged fluxes may be obtained from the plotted intensities by dividing by the beam area: 28 cm^2 for the low resolution curve and 15 cm^2 for the medium resolution curve. The sharp dips in the flux at 3.35 and 6.70 Å are respectively due to (0 0 4) and (0 0 2) Bragg reflections in the pyrolytic graphite filter. The shallower dips at 4.05 and 4.67 Å are due to

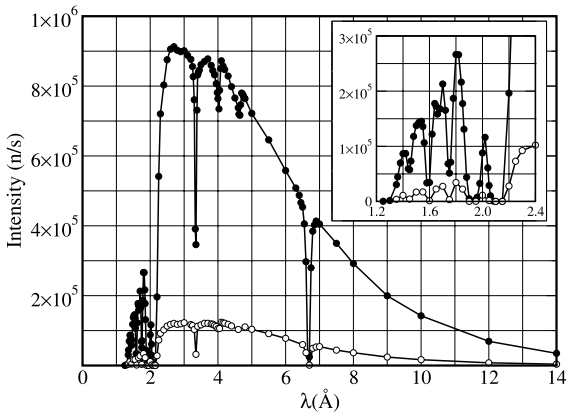

Fig. 3. The measured intensity at the DCS sample position with all choppers turning at their maximum speed. Solid and open circles represent low resolution and medium resolution measurements respectively. Lines join the points. The inset shows the short wavelength portion of the spectrum in greater detail. Error bars are smaller than the points. Beam-averaged fluxes may be calculated by dividing the plotted intensities by the beam area: 28 and 15 cm^2 for the low and medium resolution curves respectively.

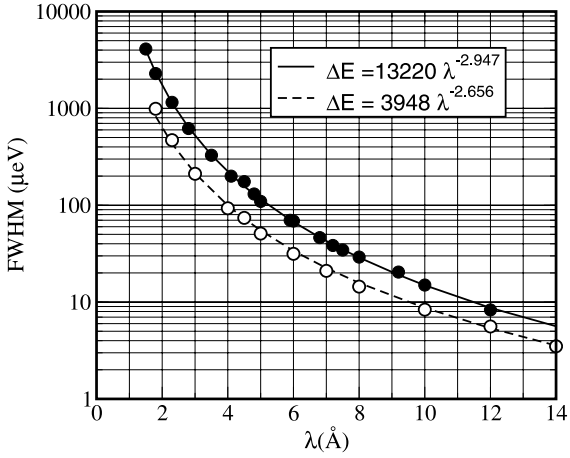

Fig. 4. Measured FWHM elastic resolution widths ΔE, with all choppers turning at their maximum speed. Solid and open circles represent low resolution and medium resolution measurements respectively. The scatter in the points is an indication of their uncertainties. Lines represent power law fits to the data, as specified in the legend.

[1] IDL is a registered trademark of Research Systems Inc.

(0 0 2) and (1 1 1) Bragg reflections respectively from aluminum components in the beam path preceding the sample. These include the cold source shell, guide windows, chopper disks, and the monochromatic beam monitor body. The complicated structure shown in the short wavelength inset is due to reflections in the crystal filter. In the low resolution mode the peak flux at the sample, roughly 3.0×10^4 n cm^{-2} s^{-1} with all choppers turning at maximum speed, occurs at about 2.7 Å. Apart from the sharp features mentioned above, there is a broad band of wavelengths from roughly 2.3 to 5.0 Å where the flux lies within 20% of the maximum value. The shape of the spectrum is slightly different for the medium resolution option.

The symbols in Fig. 4 represent measured elastic resolution widths. The lines represent power law fits to the measurements. If the elastic resolution were solely determined by the burst times of the choppers the FWHM would vary as λ^{-3}. The slower falloff with increasing wavelength suggested by the fits is caused by additional contributing factors. These factors include flight path uncertainties originating from sample size, non-zero active detector thickness, the geometry of straight detectors placed tangent to a sphere centered at the sample position, and miscellaneous engineering tolerances. At sufficiently long wavelengths these additional factors dominate the resolution width. Furthermore they become increasingly important *at any wavelength* as chopper burst times are reduced. These considerations ultimately limit the usefulness of decreasing chopper slot widths in order to gain resolution since very modest improvements in resolution are achieved at the expense of unacceptable losses in intensity.

The phase instability of the choppers is responsible for a very small contribution to the overall elastic resolution of the instrument, $\leqslant 0.2\%$ and $\leqslant 1\%$ at all available wavelengths for the low and medium resolution modes respectively.

4. Applications

To date the DCS has been used for a number of quasielastic neutron scattering (QENS) experiments, on systems such as aqueous solutions of organic molecules, hydrogen in metals, and water confined in a variety of environments. It has also been used, inter alia, for transmission and diffraction experiments, investigations of magnetic and ferroelectric materials, studies of the rotational dynamics of hydrogen, and measurements of low energy excitations in glasses. Examples of QENS experiments are briefly described in the following sections.

4.1. Water in mesoporous glasses

The dynamical behavior of water molecules confined in mesoporous silica glasses is an important topic in soft condensed matter research. Water is often found in nature within pores of nanometric dimension, e.g. on the surface of proteins, and this water can be supercooled to very low temperatures. The study of water at these temperatures is important because an understanding of its behavior under such extreme conditions is thought to be key to an explanation of the unusual properties of water under more normal conditions.

Using the DCS, Faraone et al. [13] have studied water confined in the mesoporous molecular sieves MCM-48-S and MCM-41-S. The former material has a bicontinuous structure with cubic morphology and a pore diameter of 22 Å; the latter material consists of cylindrical tubes with an inside diameter of 25 Å, arranged in a hexagonal structure. As compared with Vycor glass, which has been used in earlier studies of confined water dynamics, MCM-48-S and MCM-41-S have smaller pores and a narrower distribution of pore diameters. Both comparisons imply that these materials are better candidates than Vycor for detailed studies using the QENS technique. For the measurements of Faraone et al. [13], hydration levels were 30–35%. Data were collected at 6 Å for 0.5 mm thick flat plate samples using the medium resolution mode of operation, i.e. the medium width chopper slots. A typical spectrum, for the MCM-41-S system at 270 K, is shown in Fig. 5.

Data at four temperatures were analyzed using the relaxing-cage model [14], according to which a water molecule is trapped at short times in a cage formed by its neighbors, executing harmonic vi-

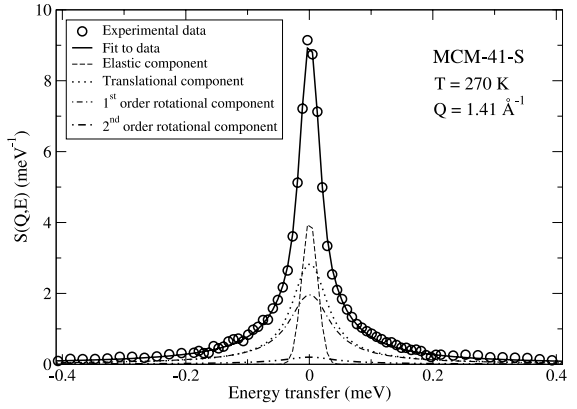

Fig. 5. Measured and calculated spectra for water in MCM-41-S at 270 K, with $Q = 1.41$ Å^{-1}. The experimental data are represented as points. The scatter in the points is an indication of their uncertainties. The overall fit to the data is shown as the solid line. Also shown are the elastic component originating from the MCM matrix and water molecules at its surface, and the first three contributions to the scattering associated with successive terms in the Sears expansion.

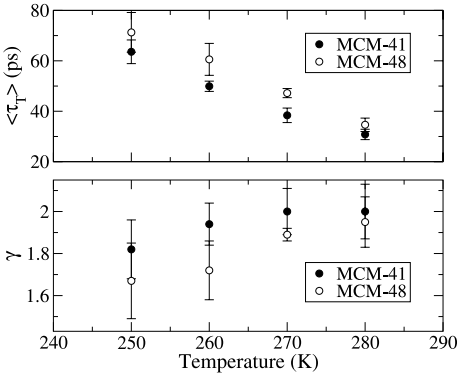

Fig. 6. The temperature dependence of the average translational relaxation time $\langle\tau_T\rangle$ and the exponent γ for water confined in two mesoporous glasses. The lengths of the error bars are one standard deviation either side of the mean.

brations and librations, whereas at longer times the cage breaks and the water molecule diffuses away. Both short time harmonic motions and long time α-relaxation are quantitatively described by this model. The intermediate scattering function $I(Q,t)$ is written as a term that is independent of time, originating from the MCM matrix and water molecules at its surface, plus a product of translational and rotational components $I_T(Q,t)$ and $I_R(Q,t)$ respectively:

$$I(Q,t) = p + (1-p)I_T(Q,t)I_R(Q,t).$$

The translational component is itself a product of terms representing short time harmonic and long time diffusional motions. In contrast the rotational component is written, following Sears [15], as an expansion in spherical Bessel functions j_ℓ:

$$I_R(Q,t) = \sum_{\ell=0}^{\infty} (2\ell+1) j_\ell^2(Qb) C_\ell(t),$$

where C_ℓ is the ℓth order rotational correlation function and $b = 0.98$ Å is the center-of-mass to hydrogen distance in water. The zeroth order correlation function is unity. The first order function is a product of short time librational and long time diffusional terms, in some ways analogous to the translational component of the intermediate scattering function. Higher order correlation functions are generated using the maximum entropy method. The end result is that the long time behavior is described by a translational relaxation time τ_0, a rotational relaxation time τ_R, and a stretched exponential coefficient β_T. Furthermore the Q dependence of the long time translational relaxation time is given by the power law relationship $\tau_T(Q) = \tau_0 Q^{-\gamma}$, where $\gamma = 2$ for diffusive motion. A result from a simultaneous fit of this model to all of the data at 270 K is shown in Fig. 5 for a single value of Q.

The fits at each temperature yield values for τ_0, τ_R, β_T, and γ. Fig. 6 shows $\langle\tau_T\rangle = (\tau_0/\beta_T)\Gamma(1/\beta_T)$, which is the average relaxation time of the stretched exponential, $\Gamma(x)$ being the gamma function. In both samples the time scales of the translational and rotational dynamics increase with decreasing temperature. The translational dynamics are somewhat slower in the MCM-48 sample, presumably because the pores are smaller. Also shown in Fig. 6 is the exponent γ, whose behavior suggests that at low temperatures the dimensionality of the diffusive motion is reduced. As the temperature is increased three-dimensional diffusive behavior is recovered.

4.2. Dynamics of proteins in solution

Proteins are long macromolecular chains consisting of amino acid repeat units that, in the

native state, adopt a well-defined and intricately folded three-dimensional conformation. The ability to predict a priori the native three-dimensional structure of an amino acid sequence, the so-called "protein folding problem", is one of the central challenges of modern-day biology and is indeed essential for the full promise of genetic therapies to come to fruition [16]; many diseases, such as Alzheimer's, bovine spongiform encephalopathy ("mad cow disease"), cystic fibrosis, and a number of cancers, result from protein folding that has gone wrong. To obtain detailed knowledge of the protein folding mechanism scientists have been investigating the properties of proteins in the native, partially unfolded and completely unfolded states, obtaining "snapshots" of the behavior of intermediates along the folding pathway. This in turn yields information that is intended to facilitate rationalization of folding mechanisms.

To improve our understanding of the molecular motions involved in protein folding, and of the role of dynamic behavior on the overall folding mechanism, Pivovar et al. [17] have used the DCS with an incident wavelength of 7.5 Å and the low resolution mode (hence roughly 35 μeV FWHM elastic energy resolution) to probe the dynamics of the electron transfer protein *cytochrome-c*. Data were collected for five different states, listed in order of increased unfolding: native, salt-induced molten globule, alkaline denatured, acid denatured and guanidine hydrochloride unfolded.

The time-of-flight data were corrected for scattering from the buffer and converted to the scattering function $S(Q,E)$; an example is shown in Fig. 7. The scattering function data were then analyzed by fitting each detector group spectrum to a model expression [18] convoluted with the instrumental resolution. The model expression is itself a convolution of terms representing motions on different time scales:

$$S(Q,E) = L(\Gamma_1) \otimes [x \cdot \delta(E) + (1-x) \cdot L(\Gamma_2)],$$

where $L(\Gamma)$ is a Lorentzian function whose FWHM is 2Γ and x is akin to an elastic incoherent structure factor. The first term is a narrow Lorentzian that describes slow motions, both bulk translation and rotational diffusion, of the entire molecule. The second term (within the square brackets) describes much faster, spatially restricted, internal (protein side-chain) motions. Thus the data were fitted to a constrained sum of Lorentzian functions with full widths Γ_1 and $\Gamma_1 + \Gamma_2$, convoluted with the instrumental resolution. Fig. 7 shows an example of a fit. The half width of the narrow Lorentzian, Γ_1, for the native state protein, is plotted as a function of Q^2 in Fig. 8. The effective global diffusion coefficients $D_{\text{eff}} = \Gamma_1/Q^2$ determined from such plots are listed in the figure in order of increased unfolding. Generally D_{eff} decreases as the protein unfolds, reflecting the correspondingly higher specific molecular volume of the non-native folding states. The exception is the acid denatured state which shows a near-native value of D_{eff}, no doubt due to strong electrostatic interactions in this system. From the widths of the broad Lorentzians, Pivovar et al. [17] also find that the time scale of the internal motions increases as a function of protein unfolding. The rather close-packed native structure is thought to provide more sharply defined short-range interactions between proximate side chains of the amino acid residues. Upon unfolding, these interactions are reduced due to the increased separation between side chains and to the presence of small, weakly interacting buffer molecules between the chains.

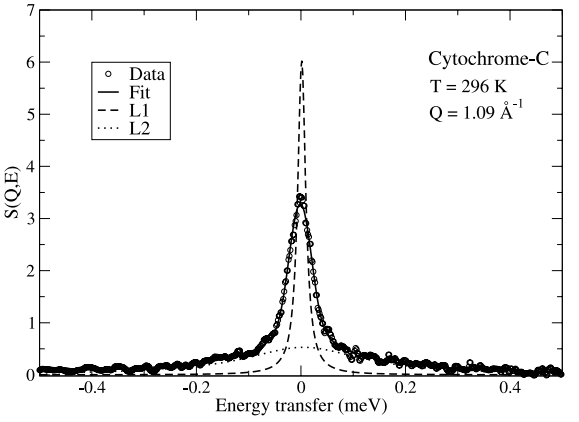

Fig. 7. Measured and calculated spectra for *cytochrome-c* at 296 K, with $Q = 1.09$ Å^{-1}. The experimental data, corrected for scattering from the buffer, are represented as points. The scatter in the points is an indication of their uncertainties. The fitted function (broadened by the instrumental resolution) is shown along with the two unbroadened Lorentzians, L1 and L2.

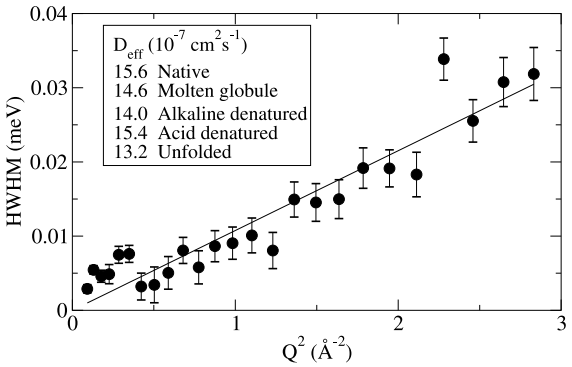

Fig. 8. The half width at half maximum height (HWHM) of the narrow Lorentzian function, fitted to native state data for *cytochrome-c* as a function of Q^2. The lengths of the error bars are one standard deviation either side of the mean. The line shows a linear fit to the data and its slope gives the effective diffusion coefficient D_{eff}. Values of D_{eff} for each of the states studied are listed.

The results of this study demonstrate the type of dynamic information that can be determined from QENS experiments performed on a protein in several different structural states. As the nature of the unfolding medium plays a critical role in the internal dynamics of the unfolded states of *cytochrome-c*, any attempts to correlate features among different folding states should take this into account. In combination with other characterization techniques, information of this sort will prove beneficial to the understanding and development of accurate protein folding mechanisms.

5. Conclusion

The DCS is the only spectrometer of its kind in North America and as such it is very popular. One of its principal strengths is its versatility in terms of choices of wavelength, resolution and intensity. Notwithstanding plans to construct a similar type of instrument at the Spallation Neutron Source in Oak Ridge, TN, the DCS is likely to remain of great interest and benefit to the neutron scattering user community for a number of years.

Acknowledgements

Many thanks to Inmaculada Peral and Yiming Qiu (University of Maryland and NCNR) for helpful discussions. We are grateful to Antonio Faraone and Sow-Hsin Chen (MIT) and to Adam Pivovar (NCNR) for figures and experimental results generously communicated prior to publication. The facilities described in this paper are supported in part by the National Science Foundation under Agreement No. DMR-0086210. Identification of commercial products does not imply recommendation or endorsement by the National Institute of Standards and Technology, nor does it imply that these products are necessarily the best for the stated purpose.

References

[1] Report on the status and needs of major neutron scattering facilities and instruments in the United States, Office of Science and Technology, Interagency Working Group on Neutron Science, June 2002, p. 49. Available from: http://www.ostp.gov/html/neutron.pdf.
[2] R.E. Williams, J.M. Rowe, Physica B 311 (2002) 117, For further information about the NCNR go to http://www.ncnr.nist.gov.
[3] N. Rosov, S. Rathgeber, M. Monkenbusch, ACS Symp. Ser. 739 (2000) 103;
see also M. Monkenbusch, R. Schaetzler, D. Richter, Nucl. Instr. Meth. A 399 (1997) 301.
[4] P.M. Gehring, D.A. Neumann, Physica B 241–243 (1998) 64; R.M. Dimeo, Z. Chowdhuri, A. Meyer, P.M. Gehring, D.A. Neumann, App. Phys. A 74 (Suppl.) (2002) S311.
[5] R.E. Lechner, F. Douchin, Y. Blanc, R. Scherm, 1973, unpublished Internal Reports of ILL Grenoble and KFA Jülich;
see also M. Bée, Quasielastic Neutron Scattering, Adam Hilger, Bristol, 1988, p. 81;
R.E. Lechner, in: Neutron Scattering in the 'Nineties, IAEA, Vienna, 1985, p. 401.
[6] S. Hautecler, E. Legrand, L. Vansteelandt, P. d'Hooghe, G. Rooms, A. Seeger, W. Schalt, G. Gobert, in: Neutron Scattering in the 'Nineties, IAEA, Vienna, 1985, p. 211.
[7] R.E. Lechner, Physica B 180&181 (1992) 973;
R.E. Lechner, R. Melzer, J. Fitter, Physica B 226 (1996) 86;
B. Rufflé, J. Ollivier, S. Longeville, R.E. Lechner, Nucl. Instr. Meth. A 449 (2000) 322.
[8] J.R.D. Copley, J. Neut. Res. 2 (1994) 95.
[9] J.R.D. Copley, J.C. Cook, Physica B 283 (2000) 386.
[10] J.R.D. Copley, Nucl. Instr. Meth. A 291 (1990) 519;
see also J.R.D. Copley, Physica B 180&181 (1992) 914.
[11] J.C. Cook, J.R.D. Copley, in preparation.
[12] J.R.D. Copley, J.C. Cook, Nucl. Instr. Meth. A 345 (1994) 313.
[13] A. Faraone, L. Liu, S.-H. Chen, C.-Y. Mou, P.-C. Shih, J.R.D. Copley, in preparation.

[14] S.-H. Chen, C. Liao, F. Sciortino, P. Gallo, P. Tartaglia, Phys. Rev. E 59 (1999) 6708;
L. Li, A. Faraone, S.-H. Chen, Phys. Rev. E 65 (2002) 041506.
[15] V.F. Sears, Can. J. Phys. 45 (1967) 237.
[16] A.R. Dinner, M. Karplus, Angew. Chem. Int. Ed. 40 (2001) 4615.
[17] A. Pivovar, M. Tarek, D.A. Neumann, unpublished results.
[18] J. Pérez, J.-M. Zanotti, D. Durand, Biophys. J. 77 (1999) 454.